Adsorption and desorption of Hg(II) from aqueous solution using magnetic Fe_3O_4@PPy composite microspheres

Xiao-qiang Cao, Fei Xiao, Xiao-yu Xie, Xuan Li, Guang Li, Lin Li, Qing-jian Zhang, Wei Zhang, Xiao-fang You, Yu-jie Gai and Xian-jun Lyu

ABSTRACT

Functional magnetic Fe_3O_4@PPy microspheres were prepared and characterized by XRD, FTIR, SEM, TEM, and magnetometer, and the adsorption of Hg(II) onto Fe_3O_4@PPy was investigated. The results showed that the adsorption of Hg(II) onto Fe_3O_4@PPy dramatically increases within 5 min and reaches adsorption equilibrium at 200 min. The adsorption of Hg(II) increases with pH increased, and a removal efficiency (*RE*) of 90.5% was obtained at pH 7.2. The isotherm studies revealed that the adsorption of Hg(II) onto the Fe_3O_4@PPy fits well with the Langmuir isotherm model, and the calculated q_m value of 232.56 mg/g. The adsorption process of Hg(II) onto the Fe_3O_4@PPy is well-fitted by the pseudo-second-order model with a high correlation coefficient (R^2) of 0.999. The thermodynamic coefficients (ΔH°, ΔS°, and ΔG°) were calculated from the temperature-dependent adsorption isotherms and illustrated that the adsorption of Hg(II) on the Fe_3O_4@PPy was spontaneous and endothermic. Different desorption agents were used to recover Hg(II) adsorbed onto Fe_3O_4@PPy, and a satisfactory recovery percentage of 93.0% was obtained by using 0.1 M HCl and 0.05 M NaCl.

Key words | adsorption, desorption, Fe_3O_4@PPy, mercury

HIGHLIGHTS

- Amino-functional magnetic Fe_3O_4@PPy microspheres were prepared and characterized.
- The Hg(II) can be adsorbed by Fe_3O_4@PPy effectively.
- The used Fe_3O_4@PPy could be regenerated by two-component desorbent of HCl and NaCl.

Xiao-qiang Cao
Fei Xiao
Xiao-yu Xie
Xuan Li
Guang Li
College of Safety and Environmental Engineering,
Shandong University of Science and Technology,
Qingdao 266590,
China

Lin Li
Xiao-fang You
Xian-jun Lyu
College of Chemical and Biological Engineering,
Shandong University of Science and Technology,
Qingdao 266590,
China

Qing-jian Zhang
Shandong Entry-exit Inspection and Quarantine Bureau,
Qingdao 266500,
China

Wei Zhang (corresponding author)
Dongying Entry-exit Inspection and Quarantine Bureau,
Dongying 257091,
China
E-mail: *weizhang19961123@163.com*

Yu-jie Gai
Qingdao Keda Mining Technology Development Co., Ltd,
Qingdao 266590,
China

doi: 10.2166/wrd.2021.080

GRAPHICAL ABSTRACT

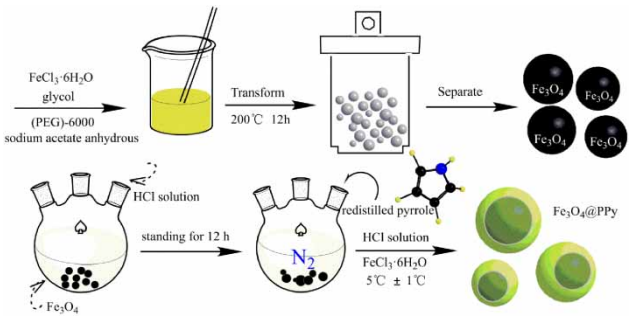

INTRODUCTION

Mercury (Hg) is considered one of the most important environmental contaminants due to its bioaccumulation and strong biological toxicity. The presence of Hg can threaten human health even at a trace level (Zhang *et al.* 2017; Zhao *et al.* 2018). For all three species of mercury (elemental (Hg^0), metallic (Hg(II)), and organic (MeHg)), Hg(II) and MeHg have higher toxicity to living organisms. Therefore, it is necessary to develop the efficient, fast, and economically feasible technology for Hg(II) removal (Yuan *et al.* 2014). Many physical, biological, and chemical techniques have been employed to remove the Hg(II) from wastewaters, such as membrane separation, ion exchange, chemical precipitation, coagulation, and adsorption (Zhang *et al.* 2012, 2020; Sharma *et al.* 2015; Wang *et al.* 2020). However, there are many problems with the current technology because of low efficiency, high cost, and complicated operation. Among these techniques, the adsorption method has been widely studied due to its low cost, simple operation, and high efficiency (Liu *et al.* 2018; Guo *et al.* 2019). Many adsorbents, such as activated carbon (Alomar *et al.* 2017; Huang *et al.* 2021), mesoporous silica (Antochshuk *et al.* 2003), chitosan (Sampaio *et al.* 2015), and magnetic nanocomposite (Kim & Park 2017; Xiao *et al.* 2019), have been used to remove the Hg(II) from the aqueous solution. Among these adsorbents, the amino-functionalized magnetic nanocomposite has gradually attracted the interest of researchers due to their superparamagnetic properties, biocompatibility, and easy to surface modification. The amino groups in nanocomposite can interact with metal ions through ion exchange or chelation and can also improve its adsorption features, such as selectivity and adsorption capacity (Zhou *et al.* 2019). The investigation of Wang *et al.* (2012) showed that the amino-functionalized magnetic composite microspheres have a good adsorption effect on the metal chromium ions in the solution. The core–shell Fe_3O_4@polypyrrole composite (Fe_3O_4@PPy) is a typical amino-functionalized magnetic nanocomposite which has been widely investigated in recent years (Peng *et al.* 2015; Tang *et al.* 2017). However, the applications of Fe_3O_4@PPy to remove Hg(II) from solution are rare.

In this work, Fe_3O_4@PPy composite microspheres are prepared and characterized by different techniques. After that, the Hg(II) adsorption behavior under different influence factors (pH, initial Hg(II) concentration, and contact time), the adsorption isotherms, kinetics, thermodynamics, and the reusability of Fe_3O_4@PPy were investigated. Finally, the optimal conditions and removal mechanism were determined.

MATERIALS AND METHODS

Chemicals and materials

$FeCl_3{\cdot}6H_2O$ (>99%), $Hg(NO_3)_2$ (>98.5%), and sodium acetate anhydrous (>99%) were purchased from Tianjin Chemical Reagent Third Factory, China. Pyrrole and glycol (>99.5%) were obtained from Shanghai Macklin Biochemical Co., Ltd, China. Absolute ethanol and

polyethylene glycol (PEG)-6000 were from Tianjin Fuyu Fine Chemical Co., Ltd, China. HCl solution (36–38%), HNO_3 (65%), and NaOH (>96%) were received from Tianjin Northern Tianyi Chemical Reagent Factory, China. All the chemicals were used without further purification. Distilled deionized water (18.4 MΩ cm) was used for material synthesis and aqueous experiments.

Methods of synthesis

Preparation of Fe_3O_4 microspheres

The Fe_3O_4 microspheres were prepared through a polyol reduction method (Peng *et al.* 2015; Figure 1). Firstly, 6 mM $FeCl_3{\cdot}6H_2O$ was dissolved in 40 mL glycol and stirred until evenly mixed. Subsequently, 42.9 mM sodium acetate anhydrous and 1.0 g of polyethylene glycol (PEG)-6000 were added and the mixed solution was stirred vigorously for 0.5 h. After that, the mixture was transferred to the 50 mL Teflon autoclave, and heated at 200 °C for 12 h. Then, the sample was collected with a permanent magnet, and washed with distilled water and ethanol. The above separation process is repeated three times. Finally, the resulting Fe_3O_4 microspheres were dried in a vacuum oven at 40 °C for 6 h.

Preparation of magnetic Fe_3O_4@PPy microspheres

Fe_3O_4 microspheres (0.10 g) were dispersed in HCl solution (40 mL, 0.1 M) under sonication, and then, the mixture was sealed in a three-necked flask and left to stand for 12 h. Subsequently, the sample was collected with the help of a magnet, washed with deionized water repeatedly to remove the residual HCl. After that, 10 mL absolute ethanol and 0.15 mL redistilled pyrrole were added into the flask under sonication and N_2 atmosphere, and then, the mixture was sealed and left to stand at 5 °C for 12 h. Then, HCl (0.165 mL, 12 M) and $FeCl_3{\cdot}6H_2O$ solution (30 mL, 1.1 M) were slowly added into the above mixture in turn under 5 ± 1 °C and N_2 atmosphere, stirring and sonication for 1 h. Finally, the precipitate was separated, washed with distilled water and ethanol, and then dried in a vacuum oven at 40 °C for 12 h (Bhaumik *et al.* 2011).

Instruments

The Fe_3O_4@PPy composite was characterized by X-ray diffraction (XRD) using Cu K_α radiation ($\lambda = 1.5406$ Å) at 45 kV/40 mA, for 2θ values between 10° and 90° (D8 Advance, Bruker, Germany). The XRD patterns obtained were analyzed by Jade 9.1 software program. The infrared

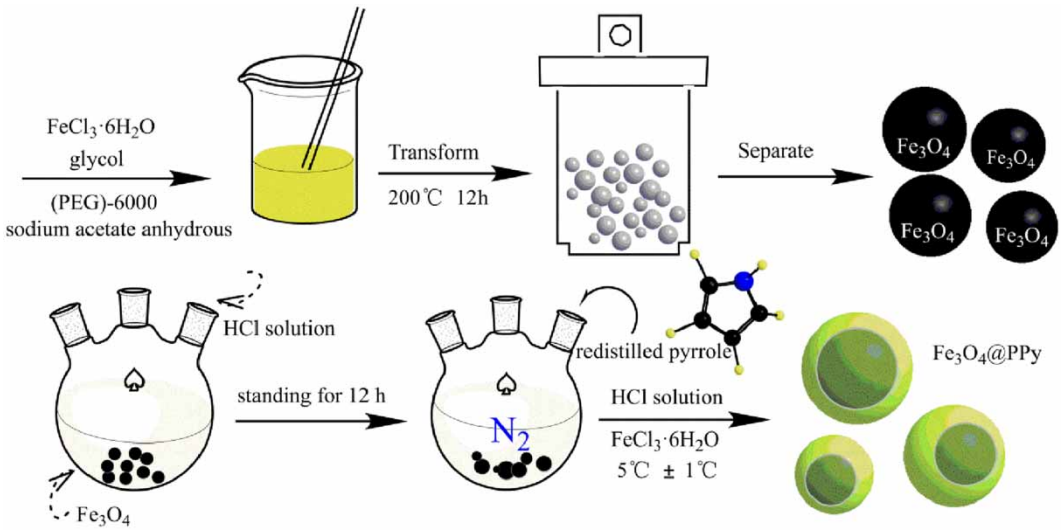

Figure 1 | The synthesis procedure of Fe_3O_4@PPy composite microspheres.

spectroscopic information was recorded by an IRPrestige-21 Fourier transform infrared spectroscopic spectrometer (FTIR, Shimadzu, Japan) for the functional group analysis. It was collected using pressed KBr discs with a resolution of 4 cm^{-1} over the range of 4,000–500 cm^{-1} on a Fourier transform infrared. The surface morphology of the composite was studied by scanning electron microscopy (SEM; Quanta 200E, FEI, USA) and transmission electron microscopy (TEM; JEM-2100F, JEOL, Japan). Magnetic measurements were performed with a superconducting quantum interference device (SQUID) magnetometer (MPMS XL-7, Quantum Design, USA). To determine Hg(II) ion removal by the adsorbent, the Hg(II) concentration in the remaining solution was measured with an inductively coupled plasma optical emission spectrometer (ICP-OES Agilent 5100, USA).

Adsorption investigation

The different concentrations (5–50 mg/L) of Hg(II)-containing solution were prepared by dissolving the $Hg(NO_3)_2$ into deionized water, and the pH was adjusted with 0.1 M HNO_3 or NaOH. For each experiment, 5 mg Fe_3O_4@PPy was dispersed into 20 mL Hg(II) solution, and then kept for a preset time (0.05–5 h) and temperature (25–45 °C). After reaching the adsorption equilibrium, the Fe_3O_4@PPy were separated with a permanent magnet, and the Hg(II) concentration in the remaining solution was analyzed using ICP-OES. The removal efficiency (*RE*) and adsorption capacity (q_e) of adsorbent are calculated using the following equations (Cao *et al.* 2020), respectively:

$$RE = \frac{c_0 - c_e}{c_0} \times 100\% \quad (1)$$

$$q_e = \frac{(c_0 - c_e)V}{m} \quad (2)$$

where q_e is the amounts of Hg(II) adsorbed (mg/g) at equilibrium, c_0 is the initial Hg(II) concentration (mg/L), c_e is the equilibrium Hg(II) concentration (mg/L), m is the mass of Fe_3O_4@PPy used (g), and V is the volume of solution (L).

Desorption investigation

1 mg Fe_3O_4@PPy with adsorbed Hg(II) ions was dispersed in 20 mL solution containing desorption agent and shaken in a conical flask for 3 h. After that, the adsorbent was separated, and the concentration of Hg(II) ions in solution was analyzed by ICP-OES for calculating Hg(II) the recovery rate.

RESULTS AND DISCUSSION

Characterization of Fe_3O_4@PPy microspheres

Figure 2 shows the XRD pattern of the Fe_3O_4@PPy microspheres. The diffraction peaks at 31.17°, 35.50°, 43.12°, 53.58°, 57.03°, and 62.63° correspond to (220), (311), (400), (511), and (440) crystal planes of the cubic anti-spinel structure, respectively. It is shown that magnetic Fe_3O_4 is not oxidized and Fe_3O_4@PPy microspheres are well crystallized in the preparation process of acidic proton and oxidative polymerization.

The FTIR spectrum of Fe_3O_4@PPy is presented in Figure 3. As shown in Figure 3, the strong absorption band at 579 cm^{-1} corresponds to the Fe–O stretching vibration of Fe_3O_4; the band at 1,556 cm^{-1} is attributed to the C = C vibrations of pyrrole rings; and the bands at 1,245, 1,033, and 773 cm^{-1} are attributed to C–N stretching vibration, C–H out-of-plane bending vibrations, and N–H in-plane bending vibrations, respectively. From these results, it can

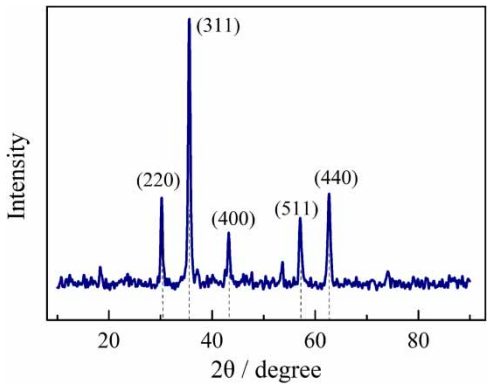

Figure 2 | XRD pattern of Fe_3O_4@PPy.

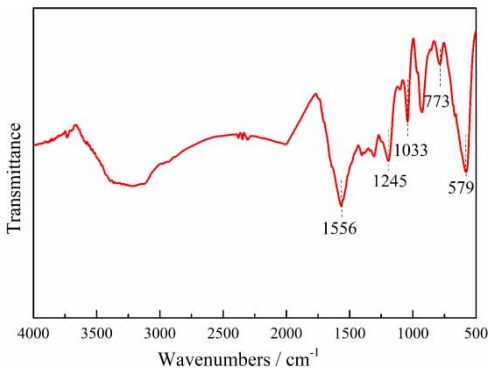

Figure 3 | FTIR spectrum of Fe_3O_4@PPy.

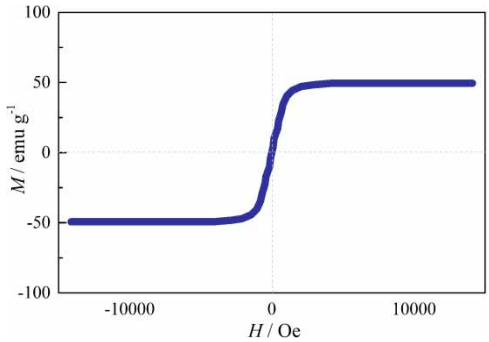

Figure 5 | Saturation magnetization curve of Fe_3O_4@PPy.

be inferred that the monomers have been polymerized successfully to be Fe_3O_4@PPy microspheres.

The SEM and TEM images of the Fe_3O_4@PPy microspheres are shown in Figure 4. From the SEM image in Figure 4, the thickness of the clear uniform shell is about 80 nm. It is clearly seen that the Fe_3O_4 core is encapsulated with polypyrrole coating, indicating the successful polymerization of pyrrole in the present reaction system and the formation of Fe_3O_4@PPy composite microspheres. It can be shown from TEM images that the Fe_3O_4@PPy microspheres with a uniform diameter size of about 290 nm have been prepared. The diameter is almost consistent with the Fe_3O_4@PPy prepared by previous study (Zhang *et al.* 2017). TEM images also show the magnification image of the Fe_3O_4@PPy microspheres retaining good dispersibility.

Figure 5 shows the saturation magnetization curves of Fe_3O_4@PPy microspheres. The saturation magnetization values of Fe_3O_4@PPy are 49.6 emu g^{-1}, and the coercive force of Fe_3O_4@PPy microspheres is 28.85 Oe, indicating that the coated microspheres have good magnetic properties (Morel *et al.* 2008).

Effect of initial Hg(II) ions concentration on Hg(II) adsorption

The effect of initial ions concentration on the adsorption of Hg(II) by Fe_3O_4@PPy is shown in Figure 6. It can be seen that the *RE* and q_e decreased and increased with initial Hg(II) concentration increasing from 5.0 to 60 mg/L, respectively. In particular, the q_e increased sharply with the initial concentration increasing from 5 to 10 mg/L; however, the adsorption capacity increased slowly at initial concentration above 20 mg/L. This phenomenon may indicate that the adsorption sites of Fe_3O_4@PPy were not

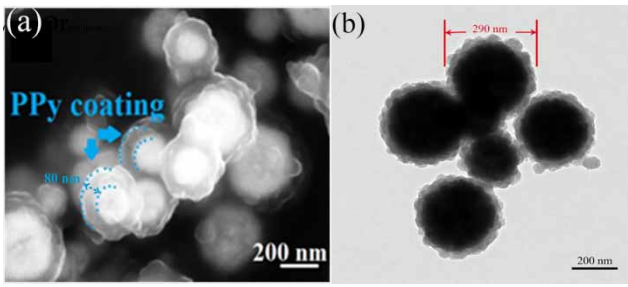

Figure 4 | SEM (a) and TEM (b) images of Fe_3O_4@PPy.

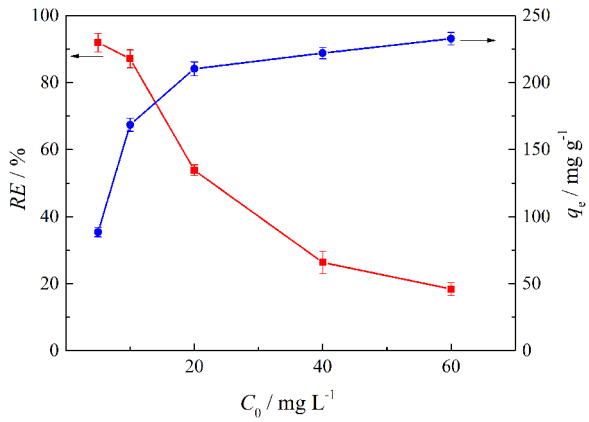

Figure 6 | Effect of initial ions concentration on the adsorption of Hg(II) by Fe_3O_4@PPy (adsorption temperature, 25 °C; adsorption time, 5 h; solution pH, 6.0; Fe_3O_4@PPy dosage, 0.25 g/L).

completely occupied at the low initial concentration of Hg(II); therefore, the adsorption capacity has not reached equilibrium. However, the number of free adsorption sites decreased with the Hg(II) ions concentration increases, resulting in part of Hg(II) ions cannot be combined with the adsorbent, and thus, the increase of q_e becomes less obvious. Li *et al.* (2019) found that a novel hierarchical carbon/Fe–Mn composite readily fabricated from biomass was utilized as an adsorbent for Hg(II) removal. The composite exhibited high removal efficiency of 96.8%, and considerable adsorption capacity of 9.8 mg/g. Zabihi *et al.* (2010) fabricated porous carbons from walnut shells, which exhibited a high monolayer adsorption capacity of 151.5 mg/g for Hg(II) removal. In the results of this study, the maximum *RE* and q_e were 93.86% and 232.55 mg/g, respectively, indicating that the Fe_3O_4@PPy can effectively adsorb the Hg(II).

Effect of the adsorbent dosage on Hg(II) adsorption

The effect of the Fe_3O_4@PPy dosage on Hg(II) removal is shown in Figure 7. As can be seen that the *RE* increases gradually with the increase of the adsorbent dosage. When the dosage is 0.25 g/L, the *RE* is 85.12%, and the *RE* reaches almost 90% at the dosage of 0.4 g/L. This phenomenon can be attributed to more available adsorption sites and the increase of adsorption contact area (Peng *et al.* 2015; Ma *et al.* 2020). On the other hand, the q_e decreased with the increase of dosage. At low dosage, the number of Hg(II) ion in solution is much more than the binding sites of adsorbents. Therefore, most adsorption sites will be occupied by Hg(II). As the dosage increases, the number of adsorption sites increases rapidly. It indicates that some adsorption sites remained in an unsaturated state on Hg(II) adsorption, resulting in a decrease in the utilization rate of the Fe_3O_4@PPy (Mollahosseini *et al.* 2019).

In a similar study to explore the effect of the adsorbent dosage on Hg(II) adsorption, Ghasemi *et al.* (2019) using polydopamine decorated SWCNTs found that the q_e of 55 mg/g and the *RE* of 82% for Hg(II) removal can be achieved at the adsorbent dosage of 0.3 g/L. Consequently, it can be concluded that Fe_3O_4@PPy nanocomposite is a more effective adsorption media for the removal of Hg(II) from aqueous solution.

Effect of solution pH on Hg(II) adsorption

The *RE* at different pHs is presented in Figure 8. As can be seen that the *RE* of Hg(II) sharply increased from ~8 to ~86% as pH was raised from 2.1 to 6.0. Furthermore, when the pH was increased from 6.0 to 7.2, the *RE* increased gradually from ~86 to ~91%. It is attributed that the amino group of the pyrrole will protonate in strong acidic solution to form positive sites such as $–NH_3^+$, resulting in electrostatic repulsion between the Hg(II) ions and the adsorbent. The dominant form of Hg(II) is in the form of stable compounds without electrostatic interaction

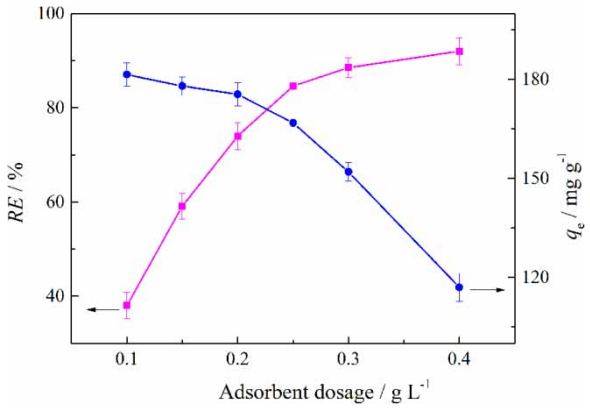

Figure 7 | Effect of the adsorbent dosage on Hg(II) adsorption (adsorption temperature, 25 °C; adsorption time, 5 h; solution pH, 6.0; initial Hg(II) concentration, 10 mg/L).

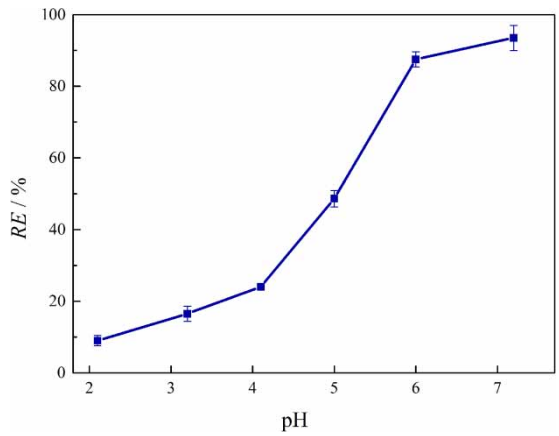

Figure 8 | Effect of pH on the Hg(II) adsorption (adsorption temperature, 25 °C; adsorption time, 5 h; initial Hg(II) concentration, 10 mg/L; Fe_3O_4@PPy dosage, 0.25 g/L).

(Zhang *et al.* 2012). Therefore, the adsorption capacity of Fe_3O_4@PPy is very low when the pH is less than 4.

At high pH, deprotonation occurred on the surface of Fe_3O_4@PPy, which reduced the electrostatic repulsion between the Hg(II) ions and the adsorbent. The amino groups of the pyrrole can combine with OH^- in the solution to form negatively charged NH_2OH, significantly enhancing the ability to adsorb Hg(II) (Deb *et al.* 2017). In the alkaline media, $Hg(OH)_3^-$ and $Hg(OH)_4^-$ complexes could be formed, which cannot be adsorbed by Fe_3O_4@PPy, because these complexes are water-insoluble (Mollahosseini *et al.* 2019).

Adsorption kinetics

The Hg(II) adsorption on Fe_3O_4@PPy was investigated as a function of contact time, and the adsorption data are analyzed by the pseudo-first-order kinetics, pseudo-second-order kinetics, and Elovich models. The linear forms of the above three models are expressed as follows (Zhang *et al.* 2019):

$$\ln(q_e - q_t) = \ln q_e - k_1 t \tag{3}$$

$$\frac{t}{q_t} = \frac{1}{k_2 q_e^2} + \frac{t}{q_e} \tag{4}$$

$$q_t = \frac{1}{b}\ln(ab) + \frac{1}{b}\ln t \tag{5}$$

where q_t (mg/g) is the amount of the Hg(II) adsorbed on Fe_3O_4@PPy at time t (min); k_1 (min^{-1}) and k_2 ($g\,mg^{-1}\,min^{-1}$) are the adsorption rate constant of pseudo-first-order and pseudo-second-order kinetics, respectively; a ($mg\,g^{-1}\,min^{-1}$) is the initial adsorption rate; and b ($g\,mg^{-1}$) is related to the extent of surface coverage and activation energy for chemisorption. The adsorption data and fitting curves are shown in Figure 9. The parameters of the three models are listed in Table 1.

As shown in Figure 9(a), the amount of Hg(II) adsorption on Fe_3O_4@PPy sharply increases within 5 min, and then reached equilibrium within approximately 200 min. The R^2 (>0.999) of the pseudo-second-order model is higher than that of two other models, and the q_e value (174.2 mg/g) is calculated from the pseudo-second-order model approximately equal to the experimental value (173.76 mg/g), indicating that the adsorption process may be chemisorption involving force through sharing or exchange of electrons between the Hg(II) and Fe_3O_4@PPy (Ghasemi *et al.* 2019). Elovich model can describe the chemisorption process on the highly heterogeneous adsorbent. The correlation coefficients of the Elovich model in this study is 0.980, indicating that there is a coordination bond between the Fe_3O_4@PPy and Hg(II) (Anbia *et al.* 2015).

Adsorption isotherms

The Langmuir, Freundlich, and D-R models were used for analyzing the adsorption data and to understand the adsorption mechanism.

The Langmuir model assumes monolayer adsorption on the homogeneous surface, and adsorption occurs at specific adsorption sites. The linear form of the Langmuir model can be expressed by the following equation (Guo *et al.* 2018):

$$\frac{c_e}{q_e} = \frac{1}{q_m \cdot K_L} + \frac{c_e}{q_m} \tag{6}$$

where K_L is Langmuir adsorption constant (L/mg), and q_m represents the maximum Hg(II) adsorption capacity of Fe_3O_4@PPy (mg/g). c_e and q_e are defined above.

The linear form of the Freundlich model can be expressed by the following equation:

$$\log q_e = \log K_F + \frac{1}{n}\log c_e \tag{7}$$

where K_F ($mg^{1-n}\,L^n\,g^{-1}$) and n are the Freundlich constants, the other parameters are defined above.

The linear form of the D-R model can be expressed as follows (Xiao *et al.* 2020):

$$\ln q_{De} = \ln q_{Dm} - \beta\varepsilon^2 \tag{8}$$

where q_{De} ($mol\,g^{-1}$) is the adsorbed molar mass of Hg(II) per gram of Fe_3O_4@PPy; q_{Dm} ($mol\,g^{-1}$) is the maximum adsorption capacity; β is the activity coefficient related to mean adsorption energy ($mol^2\,J^{-2}$); and ε is the Polanyi potential ($kJ^2\,mol^{-2}$), as can be calculated from the

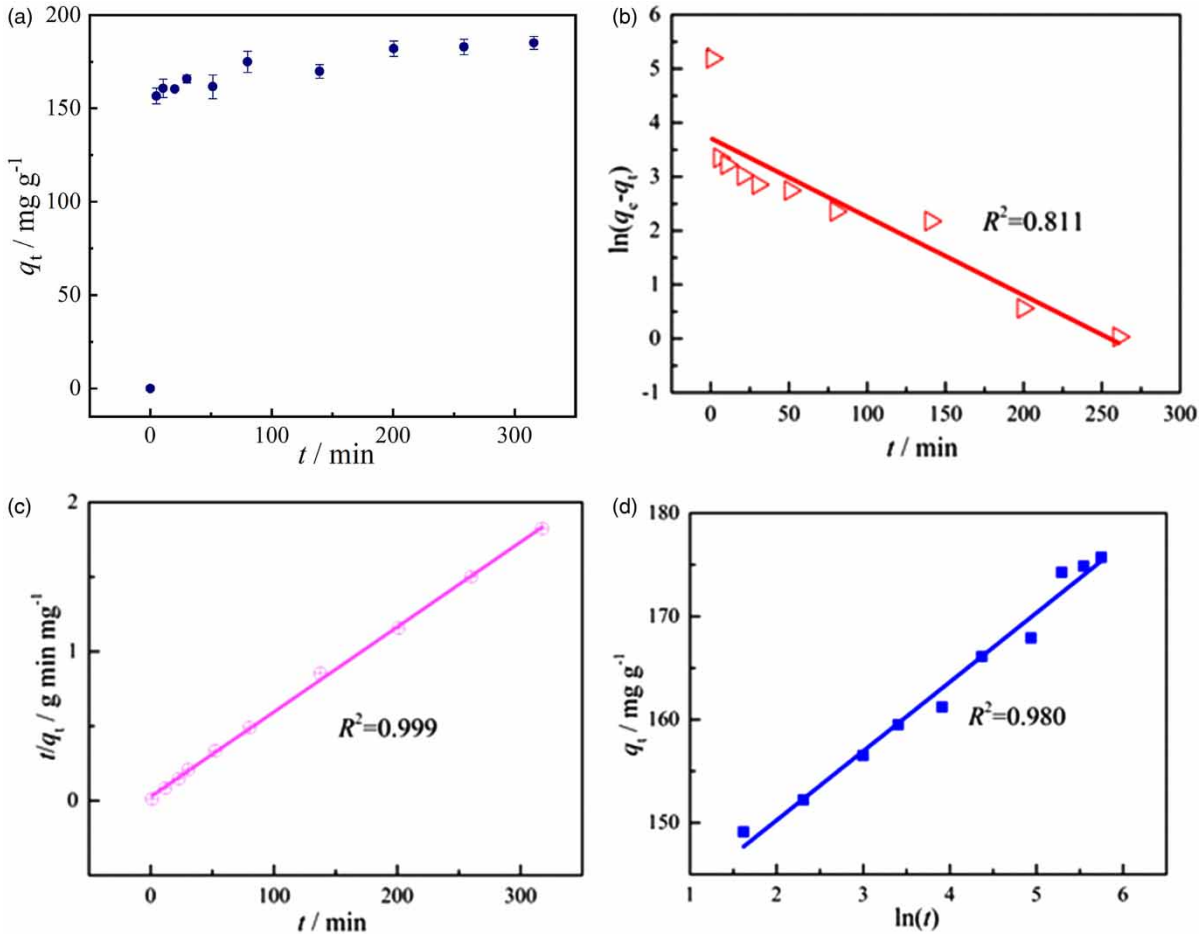

Figure 9 | Adsorption kinetics data (a) and fitted curves of pseudo-first-order kinetics (b), pseudo-second-order kinetics (c), and Elovich model (d).

Table 1 | Parameters pseudo-first-order kinetics, pseudo-second-order kinetics, and Elovich models

Pseudo-first-order			Pseudo-second-order			Elovich		
k_1	q_e	R^2	k_2	q_e	R^2	a	b	R^2
0.015	36.97	0.811	2.24×10^{-3}	174.2	0.999	4.64×10^{7}	0.160	0.980

following equation:

$$\varepsilon = RT\ln\left(1+\frac{1}{c_e}\right) \quad (9)$$

where R is the gas constant (8.314 J mol^{-1} K^{-1}) and T is the absolute temperature (K). The mean adsorption energy E (kJ mol^{-1}) can be calculated from β, and expressed as follows:

$$E = \frac{1}{(2\beta)^{0.5}} \quad (10)$$

The fitted curves and parameters of the three models are shown in Figure 10 and Table 2. The calculated R^2 values of three models indicated that the adsorption followed the

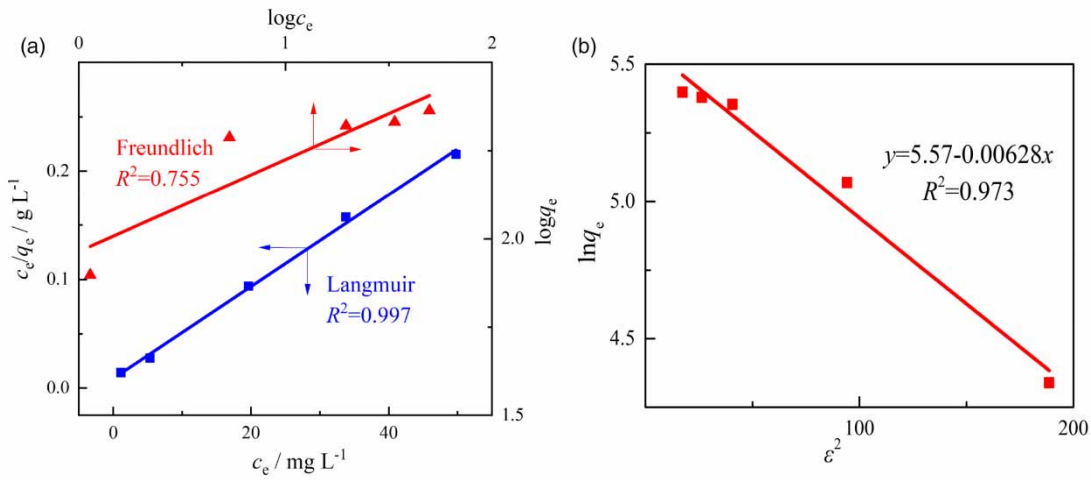

Figure 10 | The fitted curves by the Langmuir, Freundlich (a) and D-R (b) models.

Table 2 | Parameters of the Langmuir, Freundlich, and D-R models

Langmuir model			Freundlich model			D-R model		
q_m	K_L	R^2	1/n	K_F	R^2	β	E	R^2
239.76	0.614	0.997	0.258	3.31×10^5	0.755	6.0×10^{-3}	9.13	0.973

Langmuir model very well. The calculated q_m value of 239.76 mg/g is very close to the experimental value of 232.55 mg/g. The results suggested that the binding energy of the Fe_3O_4@PPy surface was uniform, namely the Fe_3O_4@PPy surface exhibited the identical adsorption activity. Generally, the E values range from 8 to 16 kJ mol^{-1} and less than 8 kJ mol^{-1} correspond to the chemical adsorption and physical adsorption mechanism, respectively (Ghasemi *et al.* 2019). The E value calculated in this study is 9.13 kJ mol^{-1}, indicating that the chemical adsorption is the dominating mechanism in the Hg(II) adsorption process.

Adsorption thermodynamics

The thermodynamic parameter can be used to determine the spontaneity of adsorption and the adsorption mechanism (Liu *et al.* 2020). The adsorption thermodynamics of Hg(II) adsorption on Fe_3O_4@PPy was investigated at 298–318 K, and the thermodynamic parameters such as the enthalpy (ΔH°), the entropy (ΔS°), and the Gibbs energy (ΔG°) are calculated by Van der Hoff equation (Equations (11)–(13)) (Zou *et al.* 2020). The experimental conditions were adsorption equilibrium time 5 h, initial Hg(II) concentration 10 mg/L, adsorbent dosage 0.25 g/L, and pH 6.0.

$$\ln K_d = \frac{\Delta S^\circ}{R} - \frac{\Delta H^\circ}{RT} \tag{11}$$

$$\Delta G^\circ = -RT \ln K_d \tag{12}$$

$$K_d = \frac{c_0 - c_e}{c_e} \cdot \frac{V}{m} \tag{13}$$

where K_d is the distribution coefficient, other parameters are defined above. The ΔG° and ΔH° can be calculated by the plot of $\ln(K_d)$ versus $1/T$ according to Equation (11), and the ΔS° can be calculated by Equation (12). The values of three parameters at different temperatures are listed in Table 3.

From Table 3, it can be seen that the values of ΔG° are more negative with temperature increasing from 298 to 318 K, indicating that the Hg(II) adsorption on Fe_3O_4@PPy is spontaneous. The positive value of ΔH° indicated that the

Table 3 | The adsorption thermodynamic parameters of Hg(II) upon Fe_3O_4@PPy

T (K)	ΔG° (kJ mol^{-1})	ΔH° (kJ mol^{-1})	ΔS° (J mol^{-1} K^{-1})
298	−2.17	40.05	141.84
303	−2.99		
308	−3.67		
313	−4.37		
318	−5.02		

adsorption process is endothermic. The positive value of ΔS° suggested that the adsorbed Hg(II) on the Fe_3O_4@PPy surface are organized in a more random fashion compared with those in the aqueous phase. Generally, the value of ΔH° for the physical and chemisorption is in the range of 2.1–20.9 kJ mol^{-1} and 80–200 kJ mol^{-1}, respectively (Li *et al.* 2019). Therefore, the adsorption of Hg(II) by Fe_3O_4@PPy has both physical adsorption and chemisorption.

Mechanism speculation

For the Hg(II) adsorption onto the Fe_3O_4@PPy, the pH is an important factor affecting adsorption by changing the species of mercury ions in the aqueous solution and Zeta potentials of Fe_3O_4@PPy. Figure 11 shows Zeta potential values and isoelectric point (IP) of Fe_3O_4@PPy. As can be seen from Figure 11, the IP value of Fe_3O_4@PPy is about 3.75. Fe_3O_4@PPy owned more negative charges and negative charges would be carried on their surface in our experimental pH 4–12, showing more potential to adsorb Hg(II) by electrostatic attraction.

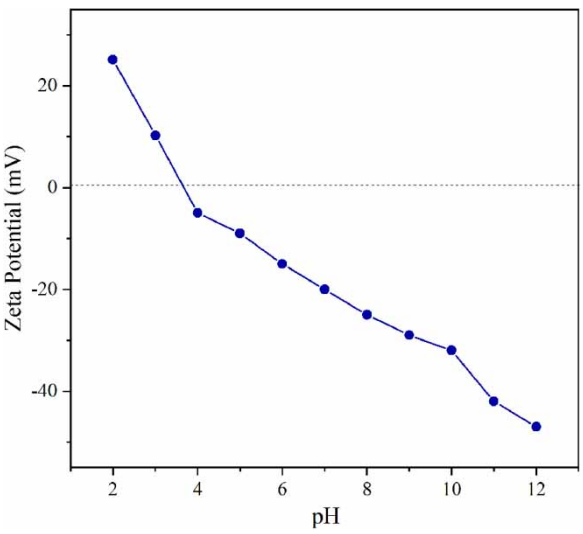

Figure 11 | Zeta potentials of Fe_3O_4@PPy under different pHs.

At pH <4, the main specie of Hg(II) in the solution is Hg^{2+}, which would compete with H^+ for adsorption sites (amino groups), as shown in Equations (14) and (15) (Yuan *et al.* 2014; Zhang *et al.* 2020). In addition, the protonation of the amino group will make a higher electrostatic repulsion between Hg(II) and Fe_3O_4@PPy (Deb *et al.* 2017). However, the part of Hg(II) can form coordinate bonds with Fe_3O_4@PPy by sharing a lone electron pair of the nitrogen atom of the amino group. Therefore, complexation is the dominating mechanism at pH <4.

$$-NH_2 + H^+ \rightarrow -NH_3^+ \quad (14)$$

$$-NH_2 + Hg^{2+} \rightarrow -NH_2Hg^{2+} \quad (15)$$

In the range of pH 4–7, $Hg(OH)^+$ and $Hg(OH)_2$ are the dominant species. The amino groups of the pyrrole can combine with OH^- in the solution to form negatively charged NH_2OH (Kim & Park 2017). Positively charged $Hg(OH)^+$ can be attracted to Fe_3O_4@PPy with negatively charged groups. On the other hand, the complexation reaction gradually increases due to the weakening of protonation (Alomar *et al.* 2017; Ghasemi *et al.* 2019). As the pH increases, the $Hg(OH)_2$ will be formed in the solution. Because $Hg(OH)_2$ is not stable, it quickly decomposes into less soluble HgO precipitation. Therefore, the adsorption mechanism has changed to the coexistence of complexation, electrostatic attraction, and precipitation removal. The reaction mechanisms are formulated as follows (Alomar *et al.* 2017; Ghasemi *et al.* 2019; Zhang *et al.* 2020):

$$2Hg^{2+} + 3OH^- + Hg^{2+} \rightarrow Hg(OH)_2 + Hg(OH)^+ \quad (16)$$

$$-NH_2 + OH^- \rightarrow -NH_2OH^- \quad (17)$$

$$-2NH_2OH^- + Hg^{2+} \rightarrow HOH_2NHgNH_2OH^- \quad (18)$$

$$Hg(OH)_2 \rightarrow HgO + H_2O \quad (19)$$

However, in the range of pH higher than 7, the insoluble complexes of $Hg(OH)_3^-$ and $Hg(OH)_4^-$ would be formed due to excess OH^-, resulting in the transformation of

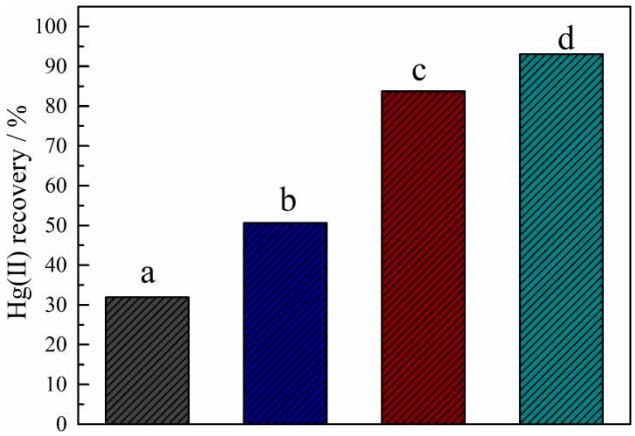

Figure 12 | Recovery efficiency of Hg(II) with different desorption agent concentrations: (a) 0.01 M HCl + 0.05 M NaCl; (b) 0.04 M HCl + 0.05 M NaCl; (c) 0.08 M HCl + 0.05 M NaCl; and (d) 0.1 M HCl + 0.05 M NaCl.

removal mechanism from adsorption to precipitation (Ghasemi *et al.* 2019). The reactions are summarized in the following equations (Ghasemi *et al.* 2019):

$$Hg(OH)_2^- + OH^- \rightarrow Hg(OH)_3^- \quad (20)$$

$$Hg(OH)_3^- + OH^- \rightarrow Hg(OH)_4^- \quad (21)$$

Desorption experiment

In order to recover mercury, avoid secondary pollution and study the reusability of Fe_3O_4@PPy, the desorption experiment was studied. The previous studies have shown that the addition of HCl will protonate Fe_3O_4@PPy (Kim & Park 2017) and makes the adsorption slower (Ghasemi *et al.* 2019; Mohammadnia *et al.* 2019). In addition, NaCl in solution will also inhibits Hg(II) adsorption because the adsorbed Hg(II) can react with Cl^- to form complexes soluble in water and the NaCl molecule can occupy the part of adsorption sites of the adsorbent (Wang *et al.* 2010). Therefore, the desorption investigation was carried out by using two-component desorbent composed of different concentrations of HCl and NaCl (0.05 M). These experimental results are shown in Figure 12.

As shown in Figure 12, the recovery rate of Hg(II) increased with the increasing concentration of HCl. The recovery rate of Hg(II) was only 31.89% with 0.01 M HCl and 0.05 M NaCl. Furthermore, the recovery rate of 93.03% can be achieved with the HCl and NaCl concentration of 0.1 and 0.05 M, respectively. The experimental results showed that the regeneration by HCl and NaCl is available, and the Fe_3O_4@PPy appeared the excellent stability and outstanding recycle possibility. The mercury desorbed in this study can be treated centrally to avoid secondary pollution of the water environment, such as making dry batteries, etc.

Comparison with other adsorbents for Hg(II) adsorption

The comparison of Hg(II) adsorption performance between Fe_3O_4@PPy and other adsorbents are listed in Table 4. It can be seen that Fe_3O_4@PPy has an excellent adsorption ability for Hg(II), indicating that Fe_3O_4@PPy has great potential in wastewater treatment applications, especially for Hg(II) removal.

Table 4 | The comparison of Hg(II) adsorption performance between Fe_3O_4@PPy and other adsorbents

	Experimental parameters					
Adsorbent	**Adsorbent dosage (mg/L)**	**Initial concentration (mg/L)**	**pH**	**Equilibrium time (min)**	**q_{max} (mg/g)**	**References**
GO/Fe_3O_4–Si–Pr–SH	200	20	7	60	129.7	Mohammadnia *et al.* (2019)
SWCNTs/Fe_3O_4@PDA	200	20	7	60	249.07	Ghasemi *et al.* (2019)
SWCNT-SH	250	30	5	60	131	Bandaru *et al.* (2013)
Carboxylate functionalized bentonite	200	25	5.5	300	113	Anirudhan *et al.* (2012)
Porous carbon	80	1	6	180	9.8	Li *et al.* (2019)
Fe_3O_4@PPy	250	10	6	200	232.55	This work

CONCLUSIONS

The magnetic Fe_3O_4@PPy composite microsphere exhibited great potential on Hg(II) ion removal from solution. The adsorption data was well fitted in the Langmuir and pseudo-second-order kinetic models, and the calculated maximum adsorption capacity was 232.56 mg/g. Thermodynamics studies show that the adsorption of Hg(II) on Fe_3O_4@PPy is an endothermic and spontaneous process, and the adsorption of Hg(II) by Fe_3O_4@PPy has both physical adsorption and chemisorption. The Hg(II) ion loaded Fe_3O_4@PPy could be regenerated by two-component desorbent composed of 0.1 M HCl and 0.05 M NaCl and the maximum recovery of 93.0% was obtained which suggested that the Fe_3O_4@PPy had good potential to capture and recover Hg(II) ion from aqueous solution.

ACKNOWLEDGEMENTS

The study was supported by the National Natural Science Foundation of China (52074176, 51774200, and 51904174); the Natural Science Foundation of Shandong Province (ZR2020ME106); 2019 Science and Technology Plan of Qingdao West Coast New District (2019-48); 'Qun xing' programs of SDUST (QX2018M43); Graduate Tutor Guidance Ability Improvement Program of Shandong Province (SDYY18080)/SDUST; Shandong Province Key Research and Development Project (2019GGX103035); and Young Science and Technology Innovation Program of Shandong Province (2020KJD001).

DATA AVAILABILITY STATEMENT

All relevant data are included in the paper or its Supplementary Information.

REFERENCES

Alomar, M. K., Alsaadi, M. A., Jassam, T. M., Akib, S. & Hashim, M. A. 2017 Novel deep eutectic solvent-functionalized carbon nanotubes adsorbent for mercury removal from water. *Journal of Colloid and Interface Science* **497**, 413–421. https://doi.org/10.1016/j.jcis.2017.03.014.

Anbia, M., Kargosha, K. & Khoshbooei, S. 2015 Heavy metal ions removal from aqueous media by modified magnetic mesoporous silica MCM-48. *Chemical Engineering Research and Design* **93**, 779–788. https://doi.org/10.1016/j.cherd.2014.07.018.

Anirudhan, T. S., Jalajamony, S. & Sreekumari, S. S. 2012 Adsorption of heavy metal ions from aqueous solutions by amine and carboxylate functionalised bentonites. *Applied Clay Science* **65–66**, 67–71. https://doi.org/10.1016/j.clay.2012.06.005.

Antochshuk, V., Olkhovyk, O., Jaroniec, M., Park, I. & Ryoo, R. 2003 Benzoylthiourea-modified mesoporous silica for mercury(II) removal. *Langmuir* **19** (7), 3031–3034. https://doi.org/10.1021/la026739z.

Bandaru, N. M., Reta, N., Dalal, H., Ellis, A. V., Shapter, J. & Voelcker, N. H. 2013 Enhanced adsorption of mercury ions on thiol derivatized single wall carbon nanotubes. *Journal of Hazardous Materials* **261**, 534–541. https://doi.org/10.1016/j.jhazmat.2013.07.076.

Bhaumik, M., Maity, A., Srinivasu, V. V. & Onyangoa, M. S. 2011 Enhanced removal of Cr(VI) from aqueous solution using polypyrrole/Fe_3O_4 magnetic nanocomposite. *Journal of Hazardous Materials* **190** (1–3), 381–390. https://doi.org/10.1016/j.jhazmat.2011.03.062.

Cao, Y. Y., Zhou, G. Z., Zhou, R. S., Wang, C. Z., Chi, B. R., Wang, Y., Hua, C. Y., Qiu, J., Jin, Y. Q. & Wu, S. 2020 Green synthesis of reusable multifunctional γ-Fe_2O_3/bentonite modified by doped TiO_2 hollow spherical nanocomposite for removal of BPA. *Science of The Total Environment* **708**, 134669. https://doi.org/10.1016/j.scitotenv.2019.134669.

Deb, A. S., Dwivedi, V., Dasgupta, K., Ali, S. M. & Shenoy, K. T. 2017 Novel amidoamine functionalized multi-walled carbon nanotubes for removal of mercury(II) ions from wastewater: combined experimental and density functional theoretical approach. *Chemical Engineering Journal* **313**, 899–911. https://doi.org/10.1016/j.cej.2016.10.126.

Ghasemi, S. S., Hadavifar, M., Maleki, B. & Mohammadnia, E. 2019 Adsorption of mercury ions from synthetic aqueous solution using polydopamine decorated SWCNTs. *Journal of Water Process Engineering* **32**, 100965. https://doi.org/10.1016/j.jwpe.2019.100965.

Guo, S. Z., Zhang, J., Li, X. L., Zhang, F. & Zhu, X. X. 2018 Fe_3O_4-CS-L: a magnetic core-shell nano adsorbent for highly efficient methyl orange adsorption. *Water Science & Technology* **77** (3), 628–637. https://doi.org/10.2166/wst.2017.602.

Guo, J. H., Yan, C. Z., Luo, Z. X., Fang, H. D., Hu, S. G. & Cao, Y. L. 2019 Synthesis of a novel ternary HA/Fe-Mn oxides-loaded biochar composite and its application in cadmium(II) and arsenic(V) adsorption. *Journal of Environmental Sciences* **85**, 168–176. https://doi.org/10.1016/j.jes.2019.06.004.

Huang, Y. M., Li, G., Li, M. Z., Yin, J. J., Meng, N., Zhang, D., Cao, X. Q., Zhu, F. P., Chen, M., Li, L. & Lyu, X. J. 2021

Kelp-derived N-doped biochar activated peroxymonosulfate for ofloxacin degradation. *Science of The Total Environment* **754**, 141999. https://doi.org/10.1016/j.scitotenv.2020.141999.

Kim, K. J. & Park, J. W. 2017 Stability and reusability of amine-functionalized magnetic-cored dendrimer for heavy metal adsorption. *Journal of Materials Science* **52** (2), 843–857. https://doi.org/10.1007/s10853-016-0380-z.

Li, Y., Xia, M. D., An, F. F., Ma, N. F., Jiang, X. L., Zhu, S. M., Wang, D. W. & Ma, J. 2019 Superior removal of Hg (II) ions from wastewater using hierarchically porous, functionalized carbon. *Journal of Hazardous Materials* **371**, 33–41. https://doi.org/10.1016/j.jhazmat.2019.02.099.

Liu, T. T., Jing, L., Liu, Q. Y. & Zhang, X. M. 2018 Facile one-pot synthesis of a porphyrin-based hydrophilic porous organic polymer and application as recyclable absorbent for selective separation of methylene blue. *Chemosphere* **212**, 1038–1046. https://doi.org/10.1016/j.chemosphere.2018.08.122.

Liu, S. R., Chen, M., Cao, X. Q., Li, G., Zhang, D., Li, M. Z., Meng, N., Yin, J. J. & Yan, B. Q. 2020 Chromium (VI) removal from water using cetylpyridinium chloride (CPC)-modified montmorillonite. *Separation and Purification Technology* **241**, 116732. https://doi.org/10.1016/j.seppur.2020.116732.

Ma, L. L., Chen, N., Feng, C. P., Li, M., Gao, Y. & Hu, Y. T. 2020 Coupling enhancement of Chromium (VI) bioreduction in groundwater by phosphorus minerals. *Chemosphere* **240**, 124896. https://doi.org/10.1016/j.chemosphere.2019.124896.

Mohammadnia, E., Hadavifar, M. & Veisi, H. 2019 Kinetics and thermodynamics of mercury adsorption onto thiolated graphene oxide nanoparticles. *Polyhedron* **173**, 114139. https://doi.org/10.1016/j.poly.2019.114139.

Mollahosseini, A., Khadir, A. & Saeidian, J. 2019 Core–shell polypyrrole/Fe_3O_4 nanocomposite as sorbent for magnetic dispersive solid-phase extraction of Al^{3+} ions from solutions: investigation of the operational parameters. *Journal of Water Process Engineering* **29**, 100795. https://doi.org/10.1016/j.jwpe.2019.100795.

Morel, A. L., Nikitenko, S. I., Gionnet, K., Wattiaux, A., Lai-Kee-Him, J., Labrugere, C., Chevalier, B., Deleris, G., Petibois, C., Brisson, A. & Simonoff, M. 2008 Sonochemical approach to the synthesis of Fe_3O_4@SiO_2 core – shell nanoparticles with tunable properties. *ACS Nano* **2** (5), 847–856. https://doi.org/10.1021/nn800091q.

Peng, X. Q., Zhang, W., Gai, L. G., Jiang, H. H., Wang, Y. & Zhao, L. C. 2015 Dedoped Fe_3O_4/PPy nanocomposite with high anti-interfering ability for effective separation of Ag(I) from mixed metal-ion solution. *Chemical Engineering Journal* **280**, 197–205. https://doi.org/10.1016/j.cej.2015.05.118.

Sampaio, C. G., Frota, L. S., Magalhães, H. S., Dutra, L. M. U., Queiroz, D. C., Araújo, R. S., Becker, H., Souza, J. R. R., Ricardo, N. M. P. S. & Trevisan, M. T. S. 2015 Chitosan/mangiferin particles for Cr(VI) reduction and removal. *International Journal of Biological Macromolecules* **78**, 273–279. https://doi.org/10.1016/j.ijbiomac.2015.03.038.

Sharma, A., Sharma, A. & Arya, R. K. 2015 Removal of mercury(II) from aqueous solution: a review of recent work. *Separation Science and Technology* **50** (9), 1310–1320. https://doi.org/10.1080/01496395.2014.968261.

Tang, S., Lan, Q., Liang, J. Y., Chen, S. R., Liu, C., Zhao, J. X., Cheng, Q., Cao, Y. C. & Liu, J. Y. 2017 Facile synthesis of Fe_3O_4/PPy core-shell magnetic nanoparticles and their enhanced dispersity and acid stability. *Materials & Design* **121**, 47–50. https://doi.org/10.1016/j.matdes.2017.02.049.

Wang, Y., Tan, H., Yang, H., Shu, H., Nie, J., Wang, T. & He, J. 2010 Effects of NaCl on Hg adsorption in soil and its kinetics. *Journal of Anhui Agricultural Sciences* **38** (25), 13750 (in Chinese).

Wang, Y. Q., Zou, B. F., Gao, T., Wu, X. P., Lou, S. Y. & Zhou, S. M. 2012 Synthesis of orange-like Fe_3O_4/PPy composite microspheres and their excellent Cr(VI) ion removal properties. *Journal of Materials Chemistry* **22** (18), 9034. https://doi.org/10.1039/C2JM30440F.

Wang, J., Wang, Q., Gao, X. L., Tian, X. X., Wei, Y. Y., Cao, Z., Guo, C. G., Zhang, H. F., Ma, Z. & Zhang, Y. S. 2020 Surface modification of mesoporous silica nanoparticle with 4-triethoxysilylaniline to enhance seawater desalination properties of thin-film nanocomposite reverse osmosis membranes. *Frontiers of Environmental Science & Engineering* **14** (1), 95–104. https://doi.org/10.1007/s11783-019-1185-5.

Xiao, X. F., Deng, Y. Y., Xue, J. L. & Gao, Y. 2019 Adsorption of chromium by functionalized metal organic frameworks from aqueous solution. *Environmental Technology* 1–13. https://doi.org/10.1080/09593330.2019.1683618.

Xiao, F., Yan, B. Q., Zou, X. Y., Cao, X. Q., Dong, L., Lyu, X. J., Li, L., Qiu, J., Chen, P., Hu, S. G. & Zhang, Q. J. 2020 Study on ionic liquid modified montmorillonite and molecular dynamics simulation. *Colloids and Surfaces A: Physicochemical and Engineering Aspects* **587**, 124311. https://doi.org/10.1016/j.colsurfa.2019.124311.

Yuan, Q., Chi, Y., Yu, N., Zhao, Y., Yan, W. F., Li, X. T. & Dong, B. 2014 Amino-functionalized magnetic mesoporous microspheres with good adsorption properties. *Materials Research Bulletin* **49**, 279–284. https://doi.org/10.1016/j.materresbull.2013.08.063.

Zabihi, M., Haghighi Asl, A. & Ahmadpour, A. 2010 Studies on adsorption of mercury from aqueous solution on activated carbons prepared from walnut shell. *Journal of Hazardous Materials* **174** (1–3), 251–256. https://doi.org/10.1016/j.jhazmat.2009.09.044.

Zhang, C., Sui, J. H., Li, J., Tang, Y. L. & Cai, W. 2012 Efficient removal of heavy metal ions by thiol-functionalized superparamagnetic carbon nanotubes. *Chemical Engineering Journal* **210**, 45–52. https://doi.org/10.1016/j.cej.2012.08.062.

Zhang, W., Zhu, W. Y., Xu, W. T., Wang, Y., Li, N., Zhang, T. T. & Wang, H. 2017 Fe_3O_4@Polypyrrole microspheres with high magnetization and superparamagnetism for efficient and fast removal of Pb (II) ions. *Russian Journal of Physical*

Chemistry A **91** (13), 2657–2665. https://doi.org/10.1134/S0036024417130258.

Zhang, H. H., Cao, X. Y., Wang, H., Ma, Z., Li, J., Zhou, L. M. & Yang, G. P. 2019 Effect of black carbon on sorption and desorption of phosphorus onto sediments. *Marine Pollution Bulletin* **146**, 435–441. https://doi.org/10.1016/j.marpolbul.2019.06.059.

Zhang, Z. Z., Xia, K., Pan, Z. W., Yang, C. X., Wang, X., Zhang, G. W., Guo, Y. F. & Bai, R. B. 2020 Removal of mercury by magnetic nanomaterial with bifunctional groups and core-shell structure: synthesis, characterization and optimization of adsorption parameters. *Applied Surface Science* **500**, 143970. https://doi.org/10.1016/j.apsusc.2019.143970.

Zhao, G. G., Ye, S. Y., Yuan, H. G., Ding, X. G., Wang, J. & Laws, E. A. 2018 Surface sediment properties and heavy metal contamination assessment in river sediments of the Pearl River Delta, China. *Marine Pollution Bulletin* **136**, 300–308. https://doi.org/10.1016/j.marpolbul.2018.09.035.

Zhou, G. Z., Wang, Y., Zhou, R. S., Wang, C. Z., Jin, Y. Q., Qiu, J., Hua, C. Y. & Cao, Y. Y. 2019 Synthesis of amino-functionalized bentonite/$CoFe_2O_4$@MnO_2 magnetic recoverable nanoparticles for aqueous Cd^{2+} removal. *Science of The Total Environment* **682**, 505–513. https://doi.org/10.1016/j.scitotenv.2019.05.218.

Zou, X. Y., Xiao, F., Liu, S. R., Cao, X. Q., Li, L., Chen, M., Dong, L., Lyu, X. J. & Gai, Y. J. 2020 Preparation and application of CPC/Keggin-al30 modified montmorillonite composite for Cr (VI) removal. *Journal of Water Process Engineering* **37**, 101348. https://doi.org/10.1016/j.jwpe.2020.101348.

First received 27 September 2020; accepted in revised form 16 December 2020. Available online 25 January 2021